THE ASTROPHYSICAL JOURNAL, 480:754–766, 1997 May 10

MODELS OF THE SPECTRAL ENERGY DISTRIBUTIONS OF FU ORIONIS STARS[1]

N. J. J. TURNER[2] AND P. BODENHEIMER
University of California Observatories/Lick Observatory and Board of Studies in Astronomy & Astrophysics, University of California, Santa Cruz, CA 95064

AND

K. R. BELL
NASA Ames Research Center, MS 245-3, Moffett Field, CA 94035
Received 1996 May 8; accepted 1996 December 9

ABSTRACT

Observed spectral energy distributions (SEDs) of FU Orionis, V1057 Cygni, and V1515 Cygni are fitted by theoretical spectra, which are calculated from models consisting of outbursting accretion disks together with flattened envelopes. Temperature in the envelopes is determined by approximate radiative equilibrium with a central source. The disk models are two-dimensional and include reprocessing of disk radiation by the disk. The theoretical spectra are calculated using a radiative transfer code and frequency-dependent opacities, at a spectral resolution of $\lambda/\Delta\lambda = 14$. Excellent matches to the data are obtained for all three objects with reasonable model parameters. Radiative transfer is also used to calculate a time series of images showing the progress of an outburst as imaged through a *B*-band filter.

Subject headings: accretion, accretion disks — radiative transfer — stars: pre–main-sequence — stars: variables: other (FU Orionis)

1. INTRODUCTION

The FU Orionis phenomenon (reviewed by Herbig 1966, 1977; Hartmann, Kenyon, & Hartigan 1993b; Hartmann & Kenyon 1996) represents a key event in the early history of a star that should provide us with important clues on the nature of pre–main-sequence stellar evolution and the formation of planetary systems. The three objects considered here are FU Orionis, which brightened by 6 mag in 120 days in 1936–1937; V1057 Cygni, which brightened by 5.5 mag in 250 days in 1969; and V1515 Cygni, which showed a much longer rise time of about 20 yr, reaching a peak about 1970. At present the three objects are respectively 1, 3, and 0.5 mag fainter than at maximum light. A recent observational summary is provided by Bell et al. (1995, hereafter BLHK).

The most likely explanation for the observed outbursts is rapid mass accretion onto the surface of a star, triggered by a thermal instability in the inner, ionized regions of a surrounding accretion disk (Paczyński 1976; Hartmann & Kenyon 1985; Lin & Papaloizou 1985). The principal physical effect that induces the instability is a heating rate, say by viscous dissipation, that increases more rapidly with temperature than does the cooling rate by radiative and convective transfer. This situation is likely to occur in the region of partial ionization of hydrogen, where the opacity is a strongly increasing function of temperature. The details of the mechanism remain to be clarified, since current models rely on an arbitrary viscous dissipation parameter (α) and in some cases on an arbitrary external perturbation. Objections have been raised, on observational grounds, to the disk model (Herbig 1989; Petrov & Herbig 1992), but by now it is clear that steady state disk models can explain a number of the observed features (Hartmann & Kenyon 1985; Adams, Lada, & Shu 1987; Kenyon, Hartmann, & Hewett 1988; Kenyon & Hartmann 1989, 1991; Calvet, Hartmann, & Kenyon 1993; Hartmann et al. 1993b). Moreover, certain features that are still difficult to explain with a model involving a disk with constant mass flux can be explained by the use of more elaborate, time-dependent, vertically resolved models (Kawazoe & Mineshige 1993; Bell & Lin 1994; BLHK).

The detailed models of BLHK, which take into account the radial and vertical structure of the disk as a function of time through a series of outbursts, form the basis of the present paper. The general picture is that the star-disk system is still at a sufficiently early stage of its evolution that matter is falling onto the outer part of the disk from the surrounding interstellar cloud (Kenyon & Hartmann 1991) at a rate $\dot{M}_{\rm in}$. The results of the calculations show that as long as $\dot{M}_{\rm in}$ exceeds $5 \times 10^{-7}\ M_\odot\ {\rm yr}^{-1}$, independent of the viscosity parameter α, the thermal ionization instability is initiated only a few stellar radii out from the star, and the disk goes into outburst. The ionization front then propagates radially through the disk on a time scale a few times longer than the local thermal value, reaching a maximum radius not larger than 0.25 AU (Bell & Lin 1994). The duration of the outburst is determined by the local viscous diffusion time in the hot, ionized region. Once this region has been sufficiently depleted by accretion onto the central star, it cools, hydrogen recombines, and the outburst declines. The interval between outbursts is determined by $\dot{M}_{\rm in}$, which controls the rate at which mass is added to the inner disk. Once the mass there has increased to the point at which the temperature once again becomes high enough to ionize hydrogen, the outburst cycle repeats. Spontaneous outbursts by this mechanism can explain the light curve of V1515 Cygni, but to explain the more rapid rise times of FU Orionis and V1057 Cygni, a small density perturbation in the inner disk is required to initiate the instability. This general explanation has been used by Lin et al. (1994) to conclude that in the case of HL Tau the value of $\dot{M}_{\rm in}$ is much larger than the accretion luminosity implied from the properties of the inner disk, so the object could be in the quiescent stage between outbursts.

[1] UCO/Lick Observatory Bulletin No. 1347.
[2] neal@ucolick.org.

The work of BLHK emphasizes comparison of models with observed light curves. In this paper, we make further tests of the viability of the detailed two-dimensional models by comparing them with observed spectral energy distributions and photometric properties. Previous work on comparison of disk models of the overall spectral energy distribution (Adams et al. 1987; Kenyon et al. 1988; Kenyon & Hartmann 1991; BLHK) have assumed that at each radius the theoretical disk radiates either the same spectrum as a blackbody at the disk surface temperature or as a stellar photosphere at the same effective temperature. A different approach is followed here. Frequency-dependent radiative transfer models are obtained from the two-dimensional disk structures (§ 2). Reprocessing of light from the hot inner disk by the cooler outer disk surface is included. Theoretical spectra are obtained as a function of the angle of inclination between the rotation axis and the line of sight (§ 3) and the differences between spectra that include reprocessing and those that do not are emphasized. The results are compared in detail (§ 4) with observations of the spectral energy distributions of the three objects in the wavelength range 0.3–100 μm. The frequency-dependent information is then used to provide a detailed calculation of the light distribution as a function of position and time for the model that fits the light curve of V1515 Cygni. The implications of the results are discussed in §5.

2. NUMERICAL DISK MODELS

In this section, we describe the disk models used to investigate the appearance of FU Orionis systems. The first component, outlined in § 2.1, is a one-dimensional, radial time-dependent set of disk evolution equations with parameters chosen in BLHK to produce an outburst with B light curves close to those observed in one of the three program objects FU Orionis, V1515 Cygni, and V1057 Cygni. A particular epoch of interest is then selected from the solution to the time-dependent equations, and the model is expanded (§ 2.2) into a set of vertical structure models at a sufficient number of radii to define $T(r, z)$ and $\rho(r, z)$, where r is the cylindrical radius and z is the height above the midplane. Reprocessing caused by the illumination of one part of the disk surface by another is found to raise surface temperatures significantly at some radii. Our method for calculating this reprocessing is described in § 2.3. When the disk is quiescent and its luminosity is low, the central star may make an important contribution (§ 2.4). Finally, in § 2.5, we add an envelope to account for the observed flat spectrum at long wavelengths. The resulting model disk, consisting of the vertical models modified by reprocessing, plus an envelope and central star, is shown schematically in Figure 1. From this structure, the spectra presented in § 4 are calculated as discussed in § 3.

2.1. *Time-dependent Models*

The outbursting disk is evolved through time by a numerical integration of a set of equations that represent the radial diffusion of disk material by viscosity. The equations are described in detail by Bell & Lin (1994) and consist of mass continuity, energy balance, and the ϕ component of the equation of motion (Bell & Lin 1994, eqs. [3]–[5]). The energy equation includes viscous heating from a Shakura & Sunyaev (1973) α viscosity, radiative losses from the surface, radial diffusion of radiation, and $P\,dV$ work. In the region of outburst, the disk is not necessarily in vertical thermal balance. The opacity used in this initial stage is the analytic approximation to the Rosseland mean opacity described in the Appendix of Bell & Lin (1994). The values of α are the same as those used by BLHK: 10^{-4} throughout most of the disk where hydrogen is neutral, and 10^{-3} in regions where the hydrogen is ionized.

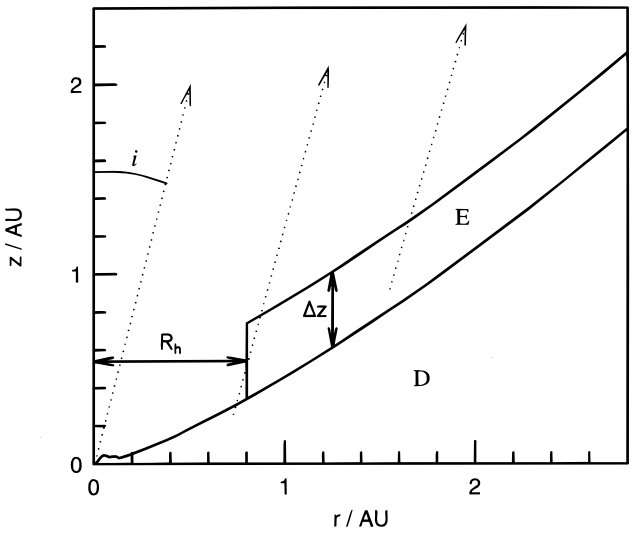

FIG. 1.—Model FU Orionis objects consist of a disk, D, and an envelope, E. The envelope has a thickness Δz and a central hole of radius R_h. The object is viewed at an angle i from pole-on. The central star is located at the lower left. Also shown are three example lines of sight along which radiative transfer is carried out.

BLHK found that the observed light curves of the three objects were fitted acceptably over a range of model parameters; these parameters include $\dot{M}_{\rm in}$ and the size and type of density perturbation to the inner disk. In this paper we choose their models A1, B1, and C1 from which to calculate detailed spectral energy distributions; the models' parameters are listed in Table 1. Outburst in the B1 disk is spontaneous, but in A1 and C1, a small perturbation is required in order to match the rapid rise times of the FU Orionis and V1057 Cygni outbursts. Such a perturbation might be provided in a clustered star-forming environment by interactions with nearby protostars. All three program objects lie in associations of young stars (see § 3.4). Alternatively, the perturbations might be caused by radial migration of protoplanets (Syer & Clarke 1996) or by time variation of the effective viscosity in the outer disk. The perturbations are annuli of material added to the radial time-dependent models during the quiescent phase between outbursts. They have inner radii r_p, masses M_p, and a fractional surface density change within the annulus of $\Delta\Sigma/\Sigma$. Outer radii are determined by M_p and $\Delta\Sigma/\Sigma$.

TABLE 1

DISK OUTBURST MODEL PARAMETERS

Star	Model	$\dot{M}_{\rm in}$ ($M_\odot$ yr^{-1})	$M_p/M_\odot$	$\Delta\Sigma/\Sigma$	$r_p/r_\odot$
FU Orionis	A1	3×10^{-6}	0.01	5	13
V1515 Cygni.....	B1	1×10^{-5}	0	0	...
V1057 Cygni.....	C1	1×10^{-6}	0.002	3	10

NOTE.—Table 2 in BLHK contains two misprints, which are corrected here.

2.2. *Vertical Structure Models*

In this subsection we discuss the sets of vertical structure models used to calculate spectra and images of the disk. The models provide the detailed distributions of temperature and density throughout the disk, $T(r, z)$ and $\rho(r, z)$. The vertical structure procedure is described in detail in Bell & Lin (1994); the essence of the program and several modifications are described here and in § 2.3.

The basic procedure is as follows:

1. Start by calculating a set of vertical structure models, for example, for model C1 of BLHK.
2. Use the resulting disk surface properties, $T_e(r)$ and $H(r)$, to calculate the flux of energy deposited at a given point by illumination from other points of the disk.
3. Add this flux at the level where Rosseland optical depth $\bar{\tau} = \frac{2}{3}$ to get a new effective temperature at each radius.
4. Calculate a new set of vertical structure models with this new boundary condition.

In the remainder of this subsection we discuss the first of these steps. The remaining three points are discussed in § 2.3.

The radial solution provides the disk effective surface temperature T_e and degree of departure from vertical thermal balance at each radius. Calculation of the vertical structure model begins near the surface of the disk. Surface pressure is chosen so as to balance the weight of the overlying atmosphere, which is otherwise ignored. In the vertical models calculated before reprocessing, the boundary lies at $\bar{\tau} = \frac{2}{3}$, while in the final vertical models from which spectra are computed (§ 2.3), it lies at $\bar{\tau} = 0.03$. Pressure and flux are next integrated toward the disk midplane. The pressure gradient balances the exact expression for the gravitational attraction of a central point mass—that is, finite disk thickness $H \approx r$ is allowed. The flux gradient includes terms due to local energy generation by viscous dissipation and transport by both mixing-length theory convection and radiative diffusion. Diffusion in the optically thin surface layer (and throughout the vertical model) is flux limited as in Bodenheimer et al. (1990), and scattering is assumed to be negligible. The opacity is the same approximation to the Rosseland mean as that used by Bell & Lin (1994), although the final vertical models use the more complete opacities discussed in § 2.3. Finally, the disk height is adjusted and the integration is repeated until it yields zero flux at the midplane.

Vertical structure models are calculated at 190 values of the radius, evenly spaced in log r from $r = 3\ R_\odot$ to $r = 158$ AU. Time-dependent models provide radial points out to $100\ R_\odot \approx 0.5$ AU. Beyond this, the disk is assumed to be transporting mass in vertical thermal balance at the rate $\dot{M}_{\rm in}$. Vertical models each consist of 100 points, with a grid adaptively spaced so as to resolve steep z gradients in temperature occurring near the surface: the gap between points is held to no more than 1/20 of the local temperature scale height $T/(\partial T/\partial z)$.

2.3. *Reprocessing*

During outbursts, models' luminosities may exceed 100 $L_\odot$, most of which is emitted by the portion of the disk inside 0.25 AU (the "inner disk"). Some fraction of the photons emitted by the inner disk is intercepted by the outer disk, heating it significantly. While the inner disk has a spectrum peaking in the visible, the outer disk is heated to temperatures such that its peak flux is at wavelengths $\lambda \geq 2$ μm. The additional flux proves useful in matching the observed fluxes at wavelengths 2–5 μm (§ 4.1). The effect of this "reprocessing" has been studied in the limit of a thin disk with central star by Adams & Shu (1986). In comparison, a disk whose surface is concave up, or flared, occupies a larger solid angle as viewed from the central source and intercepts a larger fraction of the photons (Kenyon & Hartmann 1987; Ruden & Pollack 1991). All of these calculations, however, approximate the central source by a sphere of uniform temperature.

The construction of a pseudo–two-dimensional disk, described in the previous two subsections, results in a disk surface with several local maxima as shown in Figure 2. In calculating the temperature distribution arising from reprocessing in this case, one must consider how the wrinkles hide the bright inner disk from some regions of the outer disk. The details of the numerical procedure developed to handle this problem will be discussed by Bell (1997). The calculation assumes that the disk is solid at the $\bar{\tau} = \frac{2}{3}$ surface, and radiates and absorbs like a black body. The calculation is done for the entire disk, not accounting for the presence of an envelope. The disk surface is divided into

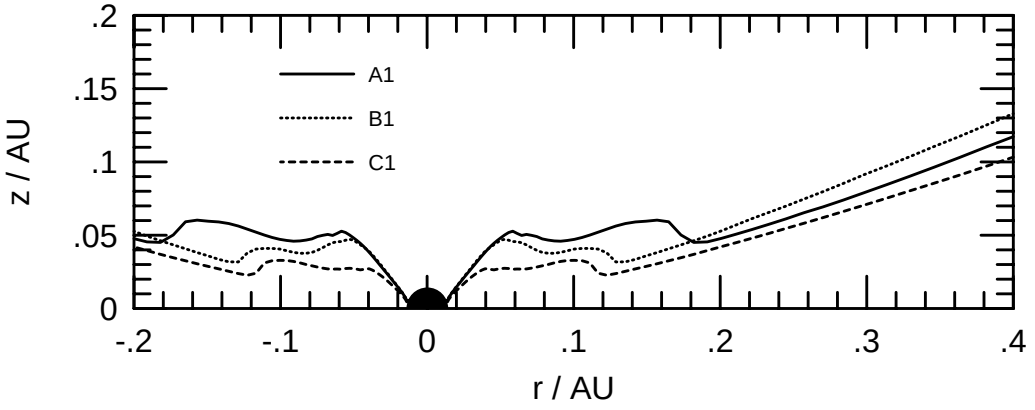

FIG. 2.—Shapes of the $\tau = 0.03$ surfaces of the inner, outbursting parts of the three disk models, showing the hot "volcanos" surrounding the central star (*black dot*). Scales on the horizontal and vertical axes are the same, so the disks are shown in their true proportions and the extent of reprocessing can be gauged.

concentric rings by cylindrical radius ω, and the rings are subdivided by equatorial angle ϕ into surface elements. To calculate the reprocessing at a point (ω_0, $\phi = 0$) on the disk surface, a line of sight is drawn to each other point (ω, ϕ). Normals to the surface at the two points are projected onto the line of sight between them. If the components are directed toward one another, there is possible mutual heating. Finally, the line of sight is traced to determine whether an intervening fold of the disk obscures the end points from one another. The sum $F_{\rm in}$ of the fluxes arriving from all emitting points determines the reprocessing temperature $T_{\rm rp}$ at the point (ω_0, 0), in balance with losses by blackbody radiation, via

$$\sigma T_{\rm rp}^4 = F_{\rm in} . \quad (1)$$

The revised effective temperature at (ω_0, 0) is then

$$T_{e,\rm tot} = (T_e^4 + T_{\rm rp}^4)^{1/4} . \quad (2)$$

New vertical structure models are next computed starting from the revised effective temperatures. Since the surface layer will be important in the radiative transfer calculation, the vertical structure calculation is now begun at an optical depth of $\bar{\tau}_0 = 0.03$. The temperature at this new starting point, T_0, is found from the effective temperature using the Eddington approximation, $T_0^4 = \frac{3}{4}T_{e,\rm tot}^4(\overline{\tau_0} + \frac{2}{3})$. If the resulting T_0 is less than the reprocessing temperature $T_{\rm rp}$, it is set equal to $T_{\rm rp}$. This approximately represents the deposition of energy into the disk atmosphere by reprocessing (calculated in detail by Calvet et al. 1991b), which was ignored in the calculation of lines of sight across the $\bar{\tau} = \frac{2}{3}$ surface. Because the flux to be reprocessed enters the disk from both above and below, the net flux through the disk surface is unchanged when reprocessing is included and in vertical thermal balance is still equal to the flux owing to viscous energy generation. Thus, the surface flux used in the calculation of the new vertical structure is still σT_e^4.

The Rosseland mean opacities used in the new vertical structure models were provided by Alexander (1995); they correspond to the frequency-dependent opacities described in § 3.1 and used in the radiative transfer calculation of § 3.2. At temperatures and densities outside the table calculated by Alexander (1995), the Rosseland mean opacities of Pollack, McKay, & Christofferson (1985) (low temperatures), Alexander, Auguson, & Johnson (1989) (higher temperatures), and Cox & Tabor (1976) (any remaining points) are used.

Temperature profiles for the B1 model with and without reprocessing are shown in Figure 3. Without reprocessing, the temperature outside the outburst region varies as $r^{-3/4}$, as in standard constant mass-flux accretion disk models. With reprocessing, there is a slight enhancement in temperature in the outburst region, inside the radius where the disk reaches a local maximum in thickness. Here, opposite sides of the disk are tilted toward one another across the central axis. We refer to this region as the "volcano." The most important effect of reprocessing, however, occurs at radii 0.1–10 AU, wherever the disk scale height is large enough so the surface sees over the near rim of the volcano to the hot region within. Because the reprocessing is set by the run of disk scale height with radius, and the scale height increases with opacity (Bell et al. 1997), the inner edge of this reprocessing region lies near the minimum in the disk thickness, which corresponds to the radius at which the temperature is just low enough for dust grains to condense. In the spectra calculated in § 4.1, only the inner edge of the reprocessing region plays a role. The rest is hidden beneath an envelope. However, the radiative equilibrium approx-

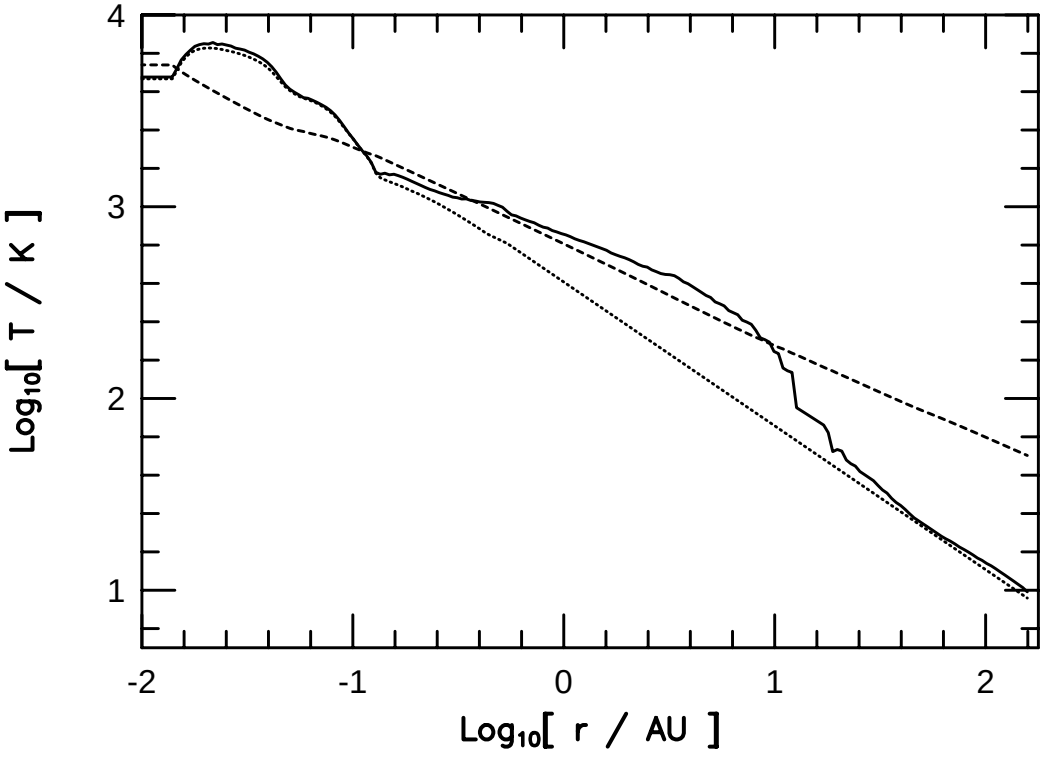

FIG. 3.—Disk temperature at the $\tau = 0.03$ surface vs. radius in the B1 model, with reprocessing (*solid line*) and without (*dotted line*). Also shown is the temperature at the base of the envelope for each radius (*dashed line*).

imation used in the envelope (§ 2.5) yields a temperature nearly continuous with that of the disk beneath, which was calculated by reprocessing for the disk alone. The match indicates that the disk surface temperatures are also approximately correct for the case where the disk is covered by the envelope. Because the envelope is optically thick, the surface temperature of the disk beneath the envelope plays no part in determining the spectral energy distribution (SED).

Over the range of radii at which reprocessing is important, the disk's temperature profile is flattened almost to $T \sim r^{-1/2}$. As one moves from the inner edge of this range to the outer, the disk height increases faster than the radius, the surface turns concave away from the midplane or "flared," and an increasing fraction of the inside of the volcano is visible from the disk surface. Beyond $r \approx 10$ AU, reprocessing is insignificant because the disk surface is concave toward the midplane and the bright inner disk is hidden from view. This change in curvature is due mostly to the opacity law $\bar{\kappa}(T)$ (Bell et al. 1997). Below the water ice condensation temperature of 125 K to which the disk material falls near 10 AU, $\bar{\kappa}$ is proportional to T^2, while in warmer material, the opacity varies more slowly with temperature.

The main change in the disk's vertical structure due to inclusion of reprocessing, apart from the rise in surface temperature, is an increase in the thickness of the surface layer. The increase is greatest at radii between 4 and 8 AU, where reprocessing thickens the disk by 10%. At the midplane, temperature and density nowhere change more than 1.6%. For this reason, the extra energy input from reprocessing is not expected to change significantly the time evolution of the radial disk model. The calculation of reprocessing and resulting new vertical structure models can in principle be iterated until the disk thickness and effective temperatures both converge. However, we limit our procedure to one pass because experimentation has shown that the bulk of the effect is achieved after a single application. As discussed above, the inner 0.1 AU, where almost all of $F_{\rm in}$ originates, is altered only slightly by the reprocessing calculation.

2.4. *Central Star*

Since the innermost radius r included in the disk models is 3 $R_\odot$, we must choose temperature and density distributions for $r < 3$ $R_\odot$. If the central star is a T Tauri star of solar mass and luminosity, its surface temperature and radius are between 3000 and 4000 K and about 3 $R_\odot$, respectively, which implies that during outburst, the star's own luminosity is negligible compared with that of the inner disk. However, the structure of the region at which the disk meets the star is not known. Does the disk engulf the star with hotter material in outburst, as suggested by the two-dimensional radiation hydrodynamic calculations of Kley & Lin (1996)? The disk model does not account accurately for the interface between disk and star. It assumes Keplerian rotation even at $r = 3$ $R_\odot$, whereas at this radius the radial pressure gradient is large, which suggests some departure from Keplerian rotation. At $r = 3$ $R_\odot$, the model disks' half-thicknesses are about 1 $R_\odot$.

As a test of the importance of the innermost 3 $R_\odot$ to the integrated spectrum during outburst, two spectra were calculated as described in § 3.2. For the first, the central 3 $R_\odot$ was occupied by a sphere of uniform surface temperature 3400 K. For the second, the vertical structure of the disk model at 3 $R_\odot$ was copied to smaller radii. The models' effective temperatures at 3 $R_\odot$ are 5000–6000 K, while their midplane temperatures are 1.0–1.2×10^5 K. The resulting spectra differ by at most 0.016 decade in flux over the entire wavelength range. In the remainder of this paper, the center of the disk is occupied by a star of temperature 3400 K and radius 3 $R_\odot$.

2.5. *Envelope*

FU Orionis stars show flux excesses at infrared wavelengths $\lambda \gtrsim 10$ μm when compared both with normal giant stars and with equilibrium dusty disks. In V1057 Cygni, the excess diminished after outburst in step with flux at B band, which suggests the 10 μm flux may be due to absorption and reemission of radiation from near the central object by material out of the plane of the disk, such as a circumstellar envelope (Kenyon & Hartmann 1991). As we have seen in § 2.3, the excess cannot be fully explained by disk reprocessing, because reprocessing does not heat the disk surface outside about 10 AU radius. For a viewer on the surface outside this radius, the outburst region is hidden by the curve of the disk.

Our simplified model of the envelope is a layer of uniform thickness, which touches the top of the disk and with a central hole exposing the inner disk (Fig. 1). This structure for the envelope is suggested by the results of two-dimensional collapse calculations, in which the density structure of matter infalling onto a disk is closer to plane-parallel than to spherical geometry, and most of the optical thickness is just above the surface of the disk (Yorke, Bodenheimer, & Laughlin 1993). Our envelope is made from material with the same opacity function as that in the disk (§ 3.1). The temperature T_d in the envelope a distance d from the center of the system is calculated assuming the envelope dust is in approximate radiative equilibrium with the object's hot inner region. That is, the rate of energy loss by radiation is balanced by the rate at which radiation from the hot region falls on the dust:

$$4\pi\sigma T_d^4 = \frac{L_{\rm il}}{4d^2}\,, \tag{3}$$

where $L_{\rm il}$ is the "illumination luminosity," the portion of the luminosity of the outbursting part of the disk that is intercepted by the envelope. This temperature distribution is correct for an optically thin medium. For an optically thick medium, equation (3) is also approximately correct. This is indicated by the radiative transfer calculations of Hartmann, Kenyon, & Calvet (1993a) for spherical optically thick envelopes around Herbig Ae/Be stars and of Kenyon, Calvet, & Hartmann (1993) for spherically symmetric protostellar envelopes in which density is proportional to $d^{-3/2}$. The variations of temperature with distance resulting from these calculations range from $T \sim d^{-0.75}$ to $T \sim d^{-0.4}$. In non–spherically symmetric models, Yorke et al. (1993) find $T \sim d^{-1/2}$ also, in both optically thick and optically thin regions. For a thin disk, $T \sim d^{-1/2}$ reduces to $T \sim r^{-1/2}$, which yields a flat λF_λ spectrum (Adams, Lada, & Shu 1988) as observed in FU Orionis objects at $\lambda \gtrsim 5$ μm.

The parameters that fix the geometry of the envelope are its thickness Δz parallel to the disk axis, the radius of the central hole R_h, and the extinction $A_V^{\rm ENV}$ through the thickness. At the inner edge of the envelope, Δz is larger than the disk thickness. Density in the envelope is chosen so as to

yield the specified extinction at temperatures between 125 and 800 K. Opacities in this temperature regime are described in § 3.1. The thickness of the disk beneath the envelope is determined including reprocessing, but because the disk thickness is changed at most 10% by reprocessing, the effect on the spectrum is negligible.

When the optical depth through the envelope is less than unity, the spectrum of the envelope appears as emission or absorption lines superposed on the spectrum of the disk. These lines, due to water ice and silicates, appear at wavelengths 3–30 μm. Such lines do not appear in spectra of FU Orionis and V1057 Cygni (Cohen 1980) (except during dimming events such as that experienced by V1057 Cygni in 1995—Wooden et al. 1995; Wooden 1996). The lines are absent from the models' spectra, provided that at each radius, the envelope has an optical depth greater than unity at wavelengths at which it and the disk beneath it contribute significantly to the integrated SED. When this condition holds, the spectrum is also insensitive to both the density in the envelope and its variation with radius. The condition is satisfied when the extinction through the envelope is uniformly above $A_V^{\rm ENV} = 100$ mag. It is satisfied almost everywhere when density varies as the inverse square root of the disk radius, with $A_V^{\rm ENV} = 100$ mag at disk radius $r = 1$ AU. Such a density distribution is obtained when a spherical $\rho \sim d^{-3/2}$ distribution is flattened vertically into a disk. The region at which the condition is not satisfied in this case is outside 25 AU, where the envelope is now optically thin at wavelengths $\gtrsim 30$ μm. Compared with the case at which the condition is satisfied throughout the envelope, this results in a spectrum that falls off more rapidly as λ increases past 30 μm. Throughout the remainder of this paper, density in the envelope is held uniform and equal to the value that results in $A_V^{\rm ENV} = 100$ mag. Resulting densities lie between 10^{-14} and 10^{-12} g cm^{-3} for the parameters listed in Table 3. Corresponding mass infall rates can be estimated using the results of the calculations of Yorke et al. (1993). Typical velocities perpendicular to the disk surface for the infalling material in their simulations are about 3 km s^{-1}. When the infalling material has a density of 10^{-14} g cm^{-3} over the inner 25 AU of the disk, this yields a mass infall rate of 10^{-5} $M_\odot$ yr^{-1}, similar to the rates used in the time-dependent disk models (Table 1).

If the model FU Orionis objects were fully self-consistent, the envelope temperature as set by $L_{\rm il}$ would be continuous with the temperature of the disk hidden beneath it. However, as Figure 3 indicates, while the temperature calculated from reprocessing agrees quite well with the dust equilibrium temperature assigned at the same radius throughout most of the disk, there is significant departure outside $r = 10$ AU, where the curve of the disk hides the hot inner regions from points on the disk surface. Here we maintain illumination of the envelope since the radiation transfer calculations of Yorke et al. (1993) indicate that in the infalling material $T \sim r^{-1/2}$, independent of the optical depth along the line of sight to the central source.

3. CALCULATION OF EMERGENT RADIATION

3.1. *Wavelength-dependent Opacities*

New opacities for use in the radiative transfer calculation were obtained from Alexander (1995), calculated as described in Alexander & Ferguson (1994) for the S92 composition (Seaton et al. 1994) with $X = 0.70$ and $Z = 0.02$. All known sources of opacity that are significant at temperatures between about 700 and 12,500 K are included. Alexander convolved monochromatic opacities with a Gaussian filter of half-width equal to 2% of the inverse wavelength because of the very broad range of wavelengths to be covered. The result is a table of opacities $\kappa_\lambda(R, T)$ averaged around 100 wavelengths λ. R is equal to $\rho/(T/10^6\ {\rm K})^3$. The 100 wavelengths are evenly spaced in log λ from 100 nm to 100 μm. Spectral resolution is thus $\lambda/\Delta\lambda = 14$, sufficient to reveal individual strong lines. For example, Hα at wavelength 656 nm is represented by one opacity value on the line and adjacent continuum values. The table has entries every 0.5 decade in R and every 0.2 decade in T, except for temperatures from 800 to 3300 K, which bracket rapid changes in opacity due to dust evaporation and ionization. Here, there are entries every 0.1 decade in T. A few points required for the radiative transfer calculations fall outside the available R and T. In these cases, we use κ_λ at the same T and the nearest available R.

Below 700 K, there are only sparse data available on the optical properties of the materials that condense as dust grains, and the opacities are less reliable. In the absence of better frequency-dependent, low-temperature opacities, Alexander's 800 K opacities are used in the present calculation down to a temperature of 125 K. These opacities include grains made of silicates, iron, amorphous carbon, and silicon carbide. Graphite is not included in the Alexander opacities, presumably because its importance in protostellar environments is controversial (Pollack et al. 1994). Yorke (1979) also provides opacities in this temperature range but for silicate grains only. Neither Yorke's data nor the extrapolated Alexander data have temperature or density dependence. The Yorke values are slightly lower than the total opacities of Alexander at most wavelengths. For temperatures of 125 K and below, water ice becomes an important source of opacity. We use the sum of Yorke's (1979) opacities due to water ice and silicates.

3.2. *Spectra*

Radiation emerging from a distribution of density $\rho(r, z)$ and temperature $T(r, z)$ is calculated by integration of the equation of radiation transfer (Mihalas 1978)

$$\frac{dI_\lambda}{d\tau_\lambda} = I_\lambda - S_\lambda \qquad (4)$$

along a set of lines of sight through the distribution. The numerical procedure is a modification of that described by Yorke (1986). The source function used is a blackbody, $S_\lambda = B_\lambda(T)$. The optical depth τ_λ is defined by $d\tau_\lambda = \kappa_\lambda \rho\, dx$, with wavelength-dependent opacity $\kappa_\lambda(\rho, T)$. Equation (4) is solved separately at each wavelength. Wavelengths used are those for which opacities are provided (§ 3.1). For a given line of sight, optical depth $\tau_\lambda = 10$ is located by integrating from the observer into the medium. The outward integration, which determines the emergent specific intensity, then begins at this point. The specific intensity I_λ is set equal to the blackbody intensity B_λ corresponding to the local temperature, and equation (4) is integrated back toward the observer. At each integration step, the step length Δx is chosen so that its optical depth $\Delta\tau_\lambda = \kappa_\lambda \rho\, \Delta x$ is at most 0.1 and also so that it is shorter than one-third of the local spatial resolution of the outburst model. If this step would leave or enter the material making up the disk or envelope,

the step length is shortened so as to end the step within $10^{-5}\ R_\odot$ of the boundary. This ensures that physically thin layers have the correct optical depth and that abrupt opacity and temperature changes near boundaries are well represented in the integration. As needed for finding the source function and opacity along the line of sight, density and temperature are linearly interpolated on the non-rectangular grid made by the series of vertical models. Opacity at each wavelength is found by interpolating in log space on the grid of densities and temperatures described in § 3.1.

The integrated spectrum of the model is calculated by summing emergent spectra over regular square grids of lines of sight. Because temperature variation in the disk occurs over small spatial scales near the star and larger scales farther away, a nested, concentric set of line-of-sight grids is used. The innermost grid is 0.2 AU across, and successive grids are 5 times wider. The outermost extends to 125 AU radius. When viewed from directly over the pole, the disk is circularly symmetric, and the grids are one-dimensional, each with 51 lines of sight along the radius. For inclination angles $0 < i < 90°$, the view of the disk is symmetric only about the plane containing the polar axis and the line of sight. In this case, each grid is two-dimensional and consists of 51 lines of sight along the radius perpendicular to the symmetry axis and 101 along the diameter parallel to the symmetry axis. The resolution on the innermost grid is 0.004 AU, or 0.85 $R_\odot$. With the disk models described here, increasing the resolution beyond this level produces negligible change in the total spectrum.

The apparent magnitude of the model in the B spectral band is calculated by integrating in wavelength the product of the spectrum F_λ and a filter transmission curve and applying the calibration between integrated flux and magnitude of Colina & Bohlin (1994). The filter transmission curve used is that tabulated by Johnson (1965).

3.3. *Images*

The same radiative transfer calculation that yields the integrated spectrum of the object also yields a spatially resolved image. Solution of the radiative transfer equation along a line of sight yields the spectrum of radiation emerging from the disk at one point. A flux is found by integrating in wavelength the product of this spectrum with a filter transmission curve. Fluxes from all the lines of sight are assembled on a grid, which makes an image of the object.

3.4. *Distances and Extinctions*

To match the absolute level of a physical model against that of an observed spectral energy distribution, we need the distance to the object and the amount of obscuring material along our line of sight. Measurements of these quantities for the three objects are collected in Table 2. The estimate of the distance to FU Orionis is taken from Murdin & Penston (1977) and that of the distance to V1057 Cygni from Straizys et al. (1989). The distance to V1515 Cygni was estimated by Racine (1968). Extinctions to the three objects were assembled by BLHK. In adding extinction to the calculated spectra, we scale the wavelength dependence of interstellar absorption (Mathis 1990) so as to obtain the desired extinction at 0.55 μm, the central wavelength of the V band.

Also in Table 2 are the luminosities of the objects and the corresponding models. The quantities listed are apparent B magnitude, dereddened B-band luminosity, and dereddened total luminosity, integrated from 0.380 to 100 μm. B-band luminosities were calculated from the apparent magnitudes assuming $R_V = A_V/E(B-V) = 3.1$. Total luminosities were calculated by integrating the spectral energy distributions of Kenyon & Hartmann (1991), assuming for V1515 Cygni a falloff at long wavelength with the same shape as that of V1057 Cygni. The models' B-band and total luminosities were calculated using the methods of § 3.2 and the parameters of Table 3. The discrepancy between the luminosities of the C1 model and V1057 Cygni was resolved by placing the C1 model at 500 pc rather than at 550 pc (see § 4.1). This lies within the uncertainty in the distance measurement. The apparent B magnitude of V1515 Cygni was found by extrapolating the light curve through a dimming that began in 1980 (Kenyon, Hartmann, & Kolotilov 1991). The B-band luminosity calculated for V1515 Cygni from the magnitude is thus not directly comparable with the total luminosity, which is calculated from a SED that includes the effects of the dimming.

4. RESULTS

4.1. *Spectral Fits*

Figure 4 shows our best matches to recent observed spectral energy distributions of the three stars. These are the data collated by Kenyon & Hartmann (1991) but without dereddening. SED points are placed at the nominal wavelengths of the photometric bands, which in most cases are effective wavelengths for equal input energy at all wavelengths. Filter transmission curves are taken from Johnson (1965) for bands $UBVRI$ and N, from Bessell & Brett (1988) for $JHKLM$, and from references under Kenyon & Hartmann (1991) for other bands. The models' parameters are given in Table 3.

Figure 4 also shows that the B1 model spectrum coincides with the V1515 Cygni data at B band and is an excellent fit at other wavelengths, if it is reddened by $A_V = 3.2$ mag instead of the nominal $A_V = 2.8$ mag. Some of the V1515 Cygni data were obtained while that object had not fully recovered from a dimming it experienced beginning in 1980. The dimming, which is thought to be a dust condensation event, was accompanied by an increase in the object's reddening (Kenyon et al. 1991).

The data in Figure 4 include measurements obtained over about 10 years, so a little caution is needed in match-

TABLE 2

DISTANCES, EXTINCTIONS, AND CURRENT-EPOCH LUMINOSITIES OF FU ORIONIS OBJECTS

STAR	DISTANCE (pc)	A_V (mag)	B MAG		$L_B/L_{B,\odot}$		$L_{tot}/L_\odot$	
			Data	Model	Data	Model	Data	Model
FU Orionis	400 ± 60	2.0	10.6	10.64	160	160	250	260
V1057 Cygni.....	550 ± 100	3.1	13.4	13.79	90	50	250	200
V1515 Cygni.....	1000 ± 200	2.8	13.7	13.59	160	170	230	290

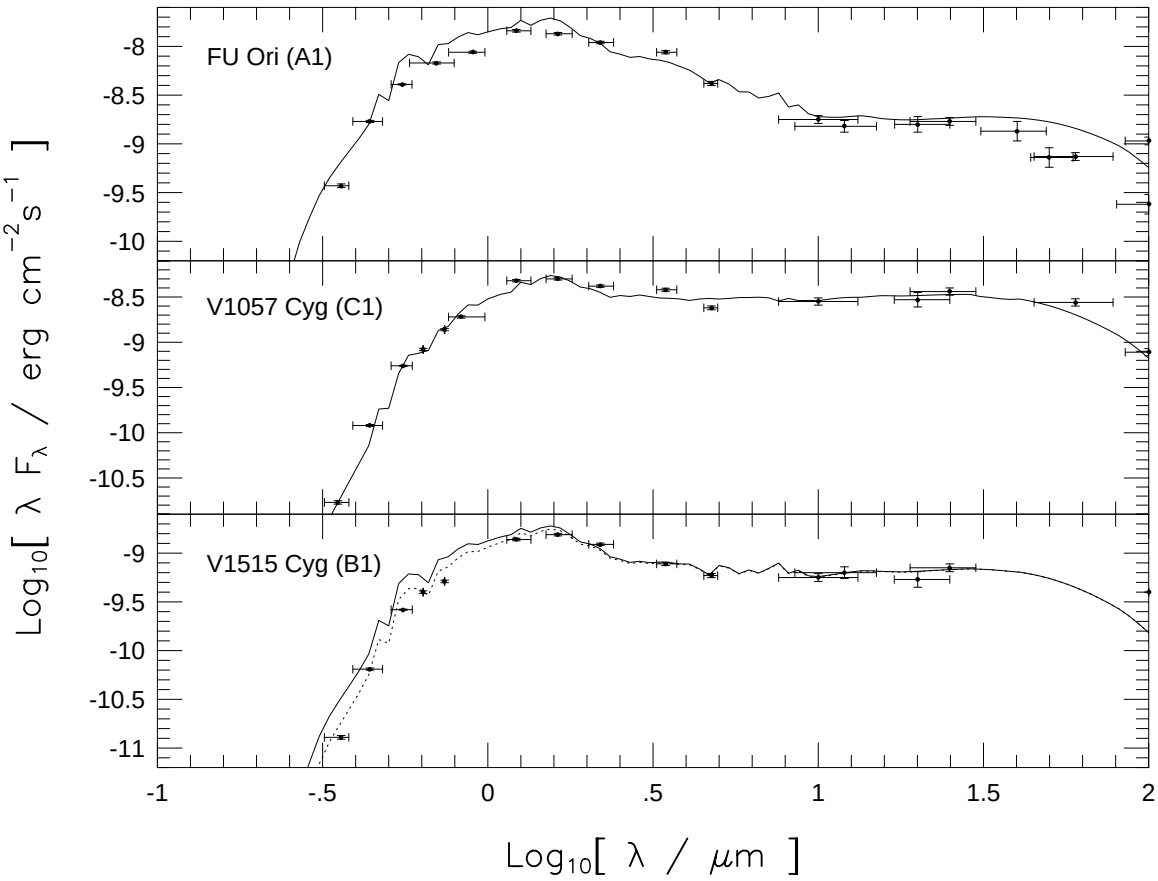

FIG. 4.—Fits (*solid lines*) to current-epoch undereddened observed fluxes from Kenyon & Hartmann (1991) (*points*) for the three objects. Vertical error bars on the data points show the quoted uncertainties in fluxes. Horizontal error bars extend to the wavelengths where filter transmission drops to 50% of its peak value. Where the wavelength range is short or the flux error is small, error bars lie inside the points. Interstellar reddening is included in the model spectra. The B1 model spectrum is also reddened an additional 0.4 mag (*dotted line*), as a possible way to allow for V1515 Cygni's sudden 1980 dimming. Parameters of the models are listed in Table 3.

ing them with models of any particular epoch. For example, points at 12, 25, 60, and 100 μm were obtained with the *Infra-Red Astronomy Satellite* (*IRAS*) in 1983–1984, while near-infrared data were obtained by Kenyon & Hartmann (1991) in 1989–1990. The spectra are calculated from models at epoch 1993.

4.2. *Comparison with Other Spectral Fits*

In this subsection, we compare the fits generated in § 4.1 with those obtained in previous attempts to model the spectral energy distributions of FU Orionis stars using accretion disks.

The models of Adams et al. (1987) are constant mass-flux accretion disks, with excess IR emission arising in dusty shells, remnant wedges of the objects' spherically symmetric parent molecular cloud cores lying $\geq$1–10 AU from the central object. A spectrum, calculated assuming blackbody emission from the disk and envelope and grain opacities in the envelope, matches the spectrum of FU Orionis adequately at visible wavelengths, but rises from 10 to 30 μm, in conflict with the data presented in Kenyon & Hartmann (1991) and plotted in Figure 4.

TABLE 3

PARAMETERS USED IN CALCULATING THE SIMULATED SPECTRA SHOWN IN FIGURE 4

Star	Model	Distance (pc)	i (deg)	$L_{il}/L_{\odot}$	R_h/AU	Δz/AU
FU Orionis	A1	400	30	11	0.8	0.8
V1057 Cygni.....	C1	500	0	30	0.1	0.1
V1515 Cygni.....	B1	1000	0	33	0.2	0.4

The models of Kenyon et al. (1988) are also constant mass-flux accretion disks but without a source of excess IR emission. Spectra are calculated by assigning each disk annulus the fluxes of a supergiant star of the same effective temperature and summing over the disk. Annuli with temperatures below 3500 K are assigned blackbody spectra. The resulting fits to FU Orionis and V1057 Cygni are adequate at wavelengths of 0.35–1 μm but are too bright by almost 1 mag at 2 μm and too faint by over 1 mag at 20 μm.

In the flared disk models of Kenyon & Hartmann (1991), a constant mass-flux disk reprocesses light from a central star. The surface of the disk is bent into a shape $H \sim r^{9/8}$, where H is the disk thickness and r is the cylindrical radius. This makes reprocessing more effective than in a flatter, standard constant mass-flux disk. Spectra are calculated as in Kenyon et al. (1988). The fluxes at 3–30 μm are higher than those from nonreprocessing disks, but in the wavelength region longward of 5 μm, which we match using a transition from disk to envelope, the best-fit flared-disk models of FU Orionis and V1057 Cygni are too bright at short wavelengths and too faint at long wavelengths. Kenyon & Hartmann (1991) also present spectra calculated from models of V1057 Cygni that include a spherically symmetric dusty envelope and a steady accretion disk. The radial optical depth of the model envelopes at wavelengths

5–50 μm is close to unity. The spectra match the observations well, except that they show broad features at 3–30 μm that do not appear in higher resolution observations of FU Orionis and V1057 Cygni (see § 2.5). Calvet, Hartmann, & Kenyon (1991a) also use model atmospheres to calculate a higher resolution spectrum for a constant mass-flux model FU Orionis disk at wavelengths 0.8–4 μm.

The SED fits in Figure 4 are more detailed in several ways than the three others just discussed. They are calculated from outbursting disk models in which the mass flux varies with radius; the models include reprocessing of disk emission by other parts of the disk, and the shape of the disk surface is consistent with the underlying accretion model. An envelope is included, based on results of hydrodynamic collapse simulations, and the SEDs are calculated from the models by radiative transfer with fairly complete frequency-dependent opacities. The more detailed calculation produces SEDs that match the observations closely, especially at wavelengths from 5 to 100 μm, where the spectrum is determined largely by the envelope. The difference between observed and model fluxes is no more than about 0.25 mag at most wavelengths, with a few points off by up to 0.75 mag.

4.3. *Parameter Sensitivity*

In the spectral fits of Figure 4, two sets of parameters vary the shape of the spectrum in two different wavelength regions. At visible and near-IR wavelengths, the flux is determined by the distribution of hot material, which is found only in the outbursting inner disk. At wavelengths longer than about 5 μm, the luminosity is dominated by large surface areas instead of high temperatures, and the flux is set by the envelope. At intermediate wavelengths, inner disk, reprocessing by the outer disk, and envelope can all be important, depending on the parameters. As discussed below, the parameter set needed to fit a spectrum is not necessarily unique.

The parameters that affect the disk portion of the spectral energy distribution are the viewing angle, i; whether reprocessing is included; the time-averaged mass flux, $\dot{M}$ and mass of the central star, M_*, to both of which the disk luminosity is proportional; and the interstellar extinction, A_V. Parameters that influence the envelope part of the SED are the luminosity $L_{\rm il}$ of the outbursting disk as seen from the envelope; the envelope extinction $A_V^{\rm ENV}$, thickness Δz, and central hole radius R_h; and the viewing angle i. Several of these parameters are restricted by data, while others are unimportant to the spectra. Among the disk spectrum parameters, M_* was set in the BLHK models to 1 $M_\odot$ for all three objects. This is based on a preoutburst spectrum of V1057 Cygni that indicates it was a T Tauri star and hence roughly of solar mass, and space density arguments that suggest FU Orionis objects cannot be precursors of high-mass stars (Herbig 1977). The mass fluxes were chosen by BLHK so the light curves of the model disks would match the observed time variation of B-band light (Table 1). Interstellar extinction is not treated as a parameter; we use the values discussed in § 3.4. The angle at which we view V1057 Cygni is restricted by rotational line broadening measurements to $i < 30°$ if the central mass is close to 1 $M_\odot$, while the inclination of FU Orionis must be $25° < i < 70°$ (Kenyon et al. 1988). We choose to view the models pole-on ($i = 0°$), except for FU Orionis, for which we assume an inclination of 30°.

Among the envelope spectrum parameters, the extinction $A_V^{\rm ENV}$ is set to 100 mag to ensure the envelope is optically thick at all wavelengths. Since the envelope has a temperature different from that of the underlying disk, an optically thin envelope would yield strong emission or absorption lines owing to water ice and silicates at wavelengths 3–30 μm. These are not observed in FU Orionis or in V1057 Cygni (Cohen 1980; Wooden 1996). Kenyon & Hartmann (1991) used an envelope extinction of 50 mag. However, the inner parts of our envelope are too hot for ice grains to exist and consequently have reduced opacity. For an envelope with $A_V^{\rm ENV} = 50$ mag, where ice is solid, the optical thickness is high, but wherever ice has sublimated, the optical thickness is less than unity at wavelengths $\lambda > 4$ μm. Increasing $A_V^{\rm ENV}$ beyond our chosen value of 100 mag has little effect on the spectra. Another envelope spectrum parameter, the luminosity $L_{\rm il}$ illuminating the envelope, is expected to be less than the total luminosity of the outburst region in the disk. Collapse calculations suggest that reasonable values for the envelope thickness Δz may lie in the range 0.1–10 AU (Yorke et al. 1993). The hole radius R_h must be at least 5 $R_\odot$ if the hole is to expose the peak surface temperature in the outbursting disk and must be 40 $R_\odot \approx 0.2$ AU if the entire outbursting region is to be visible.

Variation of the models' spectra over the remaining parameter space is illustrated in Figure 5, which sets out spectra calculated for the B1 model as follows:

Figure 5*a*: At viewing angles $i = 0$, 20°, 40°, and 60°: Increasing the viewing angle reduces the projected area of the disk, hence decreases the flux at all wavelengths. Beyond a critical angle, the inner edge of the envelope hides the central outbursting region, and the flux at visible wavelengths plummets.

Figure 5*b*: With and without reprocessing: The envelope is removed so the spectra reflect disk temperatures only. Reprocessing yields a spectrum that is almost flat at wavelengths of 3–10 μm, whereas a standard constant mass-flux accretion disk with $T \sim r^{-3/4}$ has a long-wavelength spectrum $\lambda F_\lambda \sim \lambda^{-4/3}$.

Figure 5*c*: With values of $\dot{M}M_*$ equal to one-half, once, and twice the standard value: The integrated disk luminosity is proportional to $\dot{M}M_*$. To scale luminosity L, we scale temperatures throughout the disk as $L^{1/4}$ (Lin & Papaloizou 1985). Note that this scaling does not accurately represent changes in spectral lines. Since the envelope illuminating luminosity $L_{\rm il}$ is not adjusted, the spectrum is unaffected at wavelengths longer than a few microns.

Figure 5*d*: With standard, one-third, and triple luminosities illuminating the envelope: The level of the flat spectrum is determined by the luminosity illuminating the envelope. A high $L_{\rm il}$ means a high starting temperature in the envelope's $T \sim r^{-1/2}$ and so a high flux at given wavelength.

Figure 5*e*: With holes in the envelope of the standard radius, one-third, and 3 times standard: Increasing the radius of the hole exposes more of the disk material heated by reprocessing to temperatures of 1000–1500 K. Since the envelope at the same radius is cooler, exposing more of the disk raises the flux at 2–3 μm.

Figure 5*f*: With envelopes of standard, one-third, and triple thicknesses Δz: Increasing the thickness of the envelope places the envelope's upper, visible surface further from the illuminating source. This reduces the flux from the

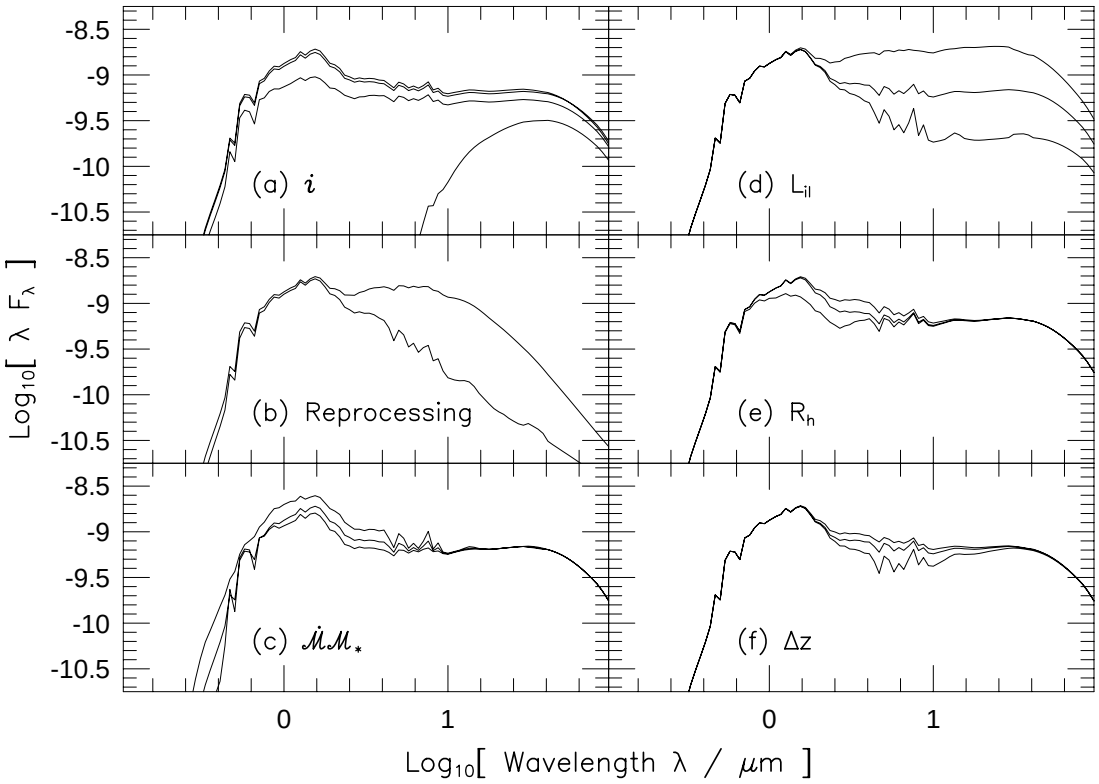

FIG. 5.—Sensitivity of the spectrum of the B1 model to three disk parameters (*left*) and three envelope parameters (*right*). The model is viewed (*a*) 0°, 20°, 40°, and 60° from pole-on (*top to bottom*); (*b*) with (*upper*) and without (*lower*) disk reprocessing (the envelope has been removed); (*c*) with disk luminosity scaled up (*top*) and down (*bottom*) by factors of 2; (*d*) with luminosity L_{il} illuminating the envelope scaled by factors of 3 (*top*) and 1/3 (*bottom*) from its best-fit value; (*e*) with the radius of the hole in the envelope varied likewise (a larger hole leads to a higher flux at 3 μm); (*f*) with the thickness of the envelope varied likewise (a thicker envelope leads to a lower flux at 3 μm). See § 4.3.

envelope at wavelength 5 μm, and total flux at this wavelength falls to near that of the disk alone. In addition, unit optical depth in the thicker envelope spans a larger range of temperatures, resulting in stronger absorption lines which are not observed in these objects.

The mapping between models and spectra is not one-to-one. There exist combinations of the parameters for which the calculated spectra are almost identical. For example, changing the distance from which we view the model multiplies the spectrum by a factor independent of wavelength, shifting it vertically on our logarithmic plots. This is almost the same as the effect of changing the angle from which we view the model, provided the viewing angle is not so large that the hot central region of the disk is obscured. Changing the mass inflow rate, $\dot{M}$, or equivalently the mass of the central star, M_*, scales the luminosity of the disk and so likewise shifts the continuous spectrum vertically. However, reasonable ranges in any of these parameters require only small changes in the accretion disk models. As the C1 model set up by BLHK is slightly less luminous than V1057 Cygni, we choose to place the model slightly closer than the star (§ 4.1). We could instead have increased its luminosity using the $M_*\dot{M}$ scaling described above under the description of Figure 5*c*. Since scaling luminosity scales the peak surface temperature of the disk, it moves the peak wavelength of the unreddened spectrum. However, once several magnitudes of interstellar reddening are applied, the peak in the λF_λ plot always lies near the H band, effective wavelength 1.63 μm, as fixed by the reddening curve.

The effects on the spectrum of the envelope hole radius R_h and thickness Δz are similar and small, and they occur in overlapping wavelength ranges. The hole radius would have almost no effect on the spectrum if our model envelope were fully consistent with the reprocessing applied to the model disk (§ 2.3), in which case the disk temperature and envelope temperature would be nearly continuous. Thus, the precise assumed geometrical structure of the envelope is not critical. For good fits to the observed spectra, the important requirements on the envelope are (1) A_V^{ENV} must be large and (2) the temperature distribution must be $r^{-1/2}$, as in equation (1).

The luminosity illuminating the envelope, L_{il}, is not degenerate with other parameters; the observed SEDs thus constrain the value of L_{il} for each object. The best-fit values listed in Table 3 are much less than the objects' total luminosities in Table 2. This occurs because equation (3) assumes isotropic radiation from the central region, whereas in fact the bulk of the total luminosity is emitted from deep inside the volcano, toward the pole, and plays no part in heating the envelope. Compared with the region inside the volcano, the portion of the inner disk that provides the chief illumination for the envelope has about twice the surface area and half the surface temperature (Figs. 2 and 3). Application of the Stefan-Boltzmann law thus suggests the envelope will be illuminated by a luminosity around one-eighth that of the total for the object. According to Tables 2 and 3, the envelope intercepts between one-sixth and one twenty-fifth of the total energy emitted by the object.

More evidence that the disk models are compatible with the required L_{il} comes from close inspection of the disk surface shapes in Figure 2. The ratio of L_{il} (Table 3) to the

total B-band luminosity of the object (which arises almost entirely in the outbursting region; Table 2) is highest for V1057 Cygni. The corresponding model, C1, has the smallest rim to its volcano, exposing hot material to the largest range of radii in the outer disk. The next highest L_{il}/L_B is exhibited by V1515 Cygni (B1). Compared with FU Orionis (A1), its rim is smaller, its outer disk surface lies higher, and its peak surface temperature occurs higher above the midplane. The three models' ranking in openness of their central volcanos is the same as the ranking of the objects in the relative luminosities L_{il}/L_B needed to explain the observed envelope spectra.

The models were truncated at a radius of 125 AU because the observed fluxes decrease with wavelength at $\lambda \gtrsim 50$ μm, which corresponds to an envelope temperature of about 60 K. The disk surface temperature at the same radius is 10 K (Fig. 3), comparable to that expected in the surrounding molecular cloud. The accretion disk model then breaks down because viscous heating is no longer the main energy input. Furthermore, radiative collapse calculations by Yorke, Bodenheimer, & Laughlin (1995) suggest that the disk plus envelope becomes optically thin near this radius. Thus, the spectra would fall off beyond this wavelength even if the models were not truncated.

4.4. *Simulated B-Band Images*

Figure 6 shows the appearance of the inner 0.3 AU of the disk in the B1 model. This is the model whose spectrum and light curve match that of V1515 Cygni, but here its envelope is removed, and it is viewed 30° from pole-on, through a B-band filter. Lighter areas of the images are brighter; the density of gray scales with the logarithm of the flux. The series of images is calculated from a series of B1 models spaced every 25 years through an outburst cycle. The series covers quiescence while material accumulates and slowly migrates in through the inner disk (1243, 1543, 1943), through onset, when the temperature at the inner edge of the disk rises high enough for hydrogen to be ionized, through the outward propagation of the ionization front (1968, 1993, 2093), and as the outburst declines (2168) and a new cycle begins (2193). Note the bright inner slope of the volcano, an asymmetric white crescent at the centers of the

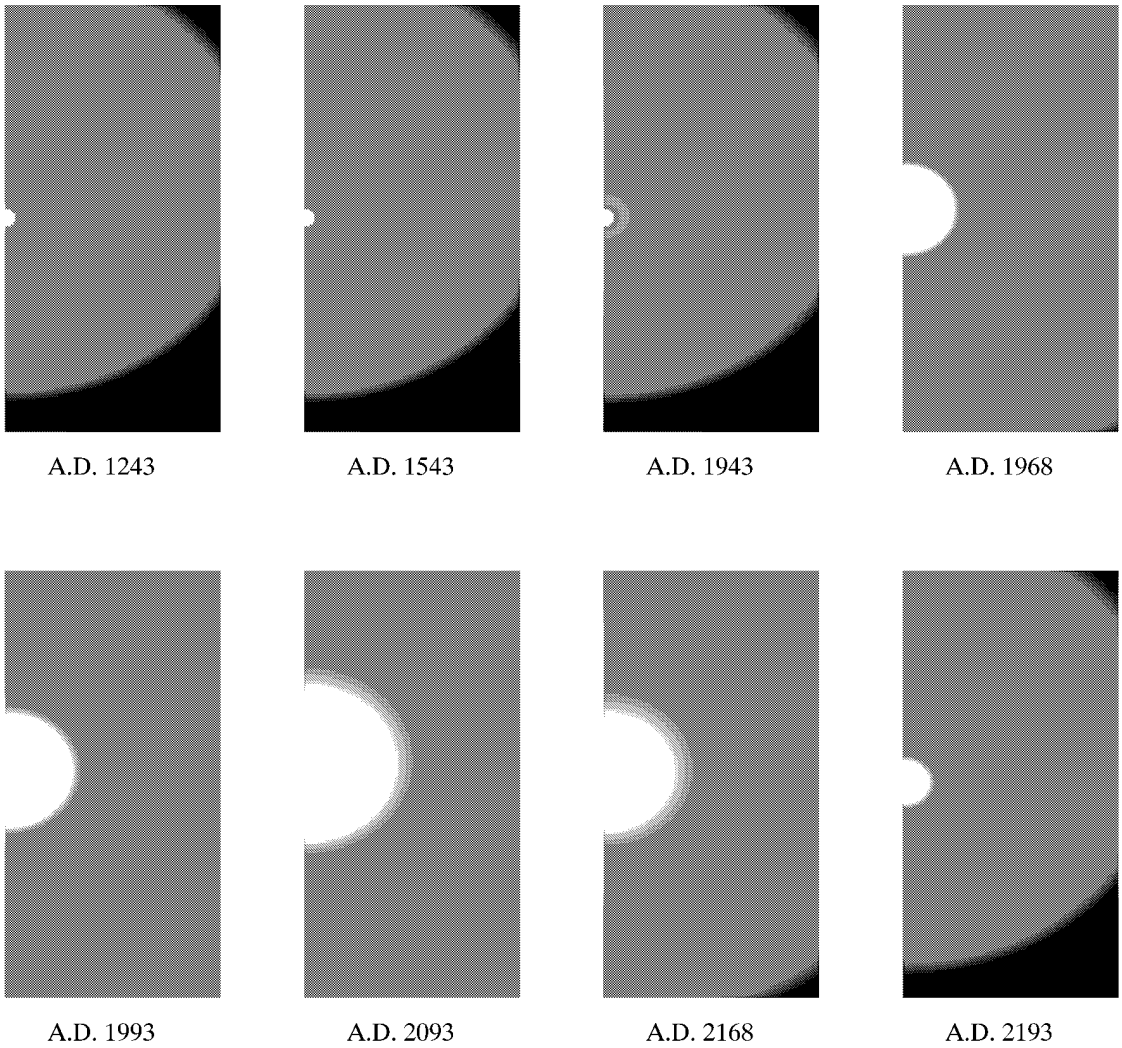

FIG. 6.—Time series showing the progress of an outburst cycle in the model V1515 Cygni (B1) disk, as seen through a B-band filter. All frames cover 0.3 AU in radius and share one flux scale that spans 18 decades. The brightest regions represent a B-band flux through the disk surface of 1×10^{11} ergs cm^{-2} s^{-1}. The disk is tipped away from the viewer by 30° from pole-on. The B1 model SED shown in Fig. 4 was calculated using the 1993 disk model in the fifth frame. A full outburst cycle in this model lasts 1150 yr.

1968, 1993, and 2093 images. Also, note the increased reprocessing in the outer disk during outburst. Reprocessing of illumination from a central star has been added to the disk models when they are quiescent. In outburst, the disk dominates total light. In quiescence, the disk is fainter than the star. The radius of the assumed star is 3 $R_\odot$, and its temperature is 3400 K. The images were computed as described in § 3.3. Though spatial scales this small in protostellar accretion disks are unlikely to be directly imaged in the near future, occultation measurements have already been used to resolve spatial scales of about 1 AU in the disk around T Tauri (Simon et al. 1996).

5. DISCUSSION AND CONCLUSIONS

In this paper, we have calculated SEDs from the outbursting accretion disk models of BLHK, using frequency-dependent radiative transfer and including disk-disk reprocessing. Previous workers have calculated SEDs for constant mass-flux disks by summing blackbody emission or stellar spectra over a $\bar{\tau} = \frac{2}{3}$ surface. Our spectra also provide a good match for the observed SEDs of FU Orionis, V1057 Cygni, and V1515 Cygni. In our model, the flux at wavelengths 0.35–2 μm is provided by the disk inside 0.25 AU. Flux at 2–5 μm is provided partly by the disk inside 0.25 AU, partly by reprocessing in the outer disk of luminosity from the inner disk and partly by a flattened envelope in approximate radiative equilibrium with a central luminosity $L_{\rm il}$. Flux at 5–100 μm is provided by the envelope.

Our model FU Orionis objects have some remaining weaknesses. Since the luminosities needed to match the envelope spectra differ somewhat from those available in the models for reprocessing by the envelope, it is likely the shape of the volcano is not accurately rendered by the disk models (§§ 2.3 and 2.4). However, among the three objects, a higher required envelope illumination luminosity does correspond to a more open model volcano (§ 4.3). Another hint of mild inaccuracies in the disk models comes from Figure 4, where both A1 and B1 show excesses at 0.55 μm over the corresponding measured fluxes. While the B1 excess may be due to the 1980 dimming event in V1515 Cygni (§ 4.1), both excesses might also be removed if the steep shapes of the volcanos shown in Figure 2 were relaxed, which would reduce the small degree of reprocessing between the volcanos' opposite walls. Whether this relaxation is realistic could be demonstrated using two-dimensional hydrodynamic simulations of the outburst region, which would allow radial derivatives of the physical quantities to act on the structure. The volcanos would be flatter also if the viscosity parameter α in the outburst region were larger than the value of 10^{-3} used in the BLHK models. The disk models further omit the back reaction of self-illumination on the propagation of the outburst, which is expected to be a second-order effect. Again in Figure 4, the spectrum of the C1 model is about 0.1 decade too faint at 3 μm and 0.1 decade too bright at 5 μm. If the model were more luminous or if its volcano were more open, so that reprocessing were stronger, this misfit might be corrected by increasing the radius of the hole in the envelope.

The model envelope is another area where further work is needed. Our model is an oversimplification chosen for the small number of parameters it introduces. Model envelopes could be generated using a two-dimensional radiation hydrodynamic collapse calculation, but the exploration of parameter space needed to find envelopes appropriate for the spectra would make this a large undertaking. However, reconciliation of the illumination luminosities with the central luminosities of the objects does require more realistic vertical density gradients in the envelope, such as would be obtained from collapse calculations.

The disk models assume a constant, low-viscosity parameter $\alpha = 10^{-4}$ outside the outburst region. As discussed by BLHK, this small viscosity results in a disk that is self-gravitating for the given input mass fluxes at radii beyond about 1 AU, yet we extend the disks to radii of 100 AU and more. This clear inconsistency is perhaps justified because outside a radius R_h (0.8 AU in the largest case, the A1 model), the disk is invisible, hidden beneath the envelope. The thickness of the outer disk does affect the spectrum via the envelope temperature, which is a function of distance from the central object (eq. [3]). But this distance is only a weak function of the disk thickness, so any effect on the spectrum is small. The other requirement on the outer disk by the outburst model is that the outer disk supply mass at a near-constant rate; the mechanism of mass transport there might for example be gravitational instability, rather than that in the standard Shakura & Sunyaev (1973) accretion disk picture.

Although the process that triggers the rapid rise-time outbursts of FU Orionis and V1057 Cygni is still not understood, work in this paper lends solid additional support to the hypothesis that a thermal accretion event in a protostellar disk is responsible for the outburst. The spectral fitting also shows that an optically thick dusty envelope is an important component of the system, required to fit the 5–100 μm region. The presence of the envelope underscores the relative youth of these objects. The calculations demonstrate that reprocessing of disk light by the disk itself can produce a surface temperature distribution $T \sim r^{-1/2}$, which would result in a flat spectrum in the (λ, λF_λ) diagram even without the envelope. However, this effect is cut off when the disk surface becomes concave toward the midplane. This occurs at a radius of about 10 AU, where the temperature at the surface $\bar{\tau} = \frac{2}{3}$ reaches the ice condensation point. As a result, the envelope is still needed to explain the flat spectrum over the full observed range of wavelengths.

Finally, we note that many more details of the mechanism powering FU Orionis outbursts can be extracted from time-resolved spectroscopic observations. Though available data are sparse, it is already known that various spectral features appear and disappear during the evolution of the individual objects. Useful in the future would be spectra from 0.1 to 100 μm, spaced in time to resolve rapid changes in the light curve. For example, BBW 76 is a recently discovered FU Orionis object that is currently fading (Eislöffel, Hessman, & Mundt 1990; Reipurth 1991). Once a light curve is available covering a sufficient fraction of an outburst, a disk model can be constructed for this object. Comparison of SEDs calculated from the model against those observed over time will provide an even more rigorous test of the validity of the outbursting accretion disk model.

These calculations were possible because David Alexander graciously calculated for us the frequency-dependent opacities. Scott Kenyon was quick to answer our questions. We also learned from discussions with Pat Cassen, Martin Cohen, Doug Lin, and Diane Wooden, and the recommen-

dations of an anonymous referee. The work was supported by grants NAGW-3408 and NAGW-4456 from the NASA Origins of Solar Systems Program and by a special NASA theory program that supports a joint Center for Star Formation Studies at NASA-Ames Research Center, University of California, Berkeley, and University of California, Santa Cruz. The research made use of NASA's Astrophysics Data System Abstract Service and the SIMBAD database, operated at CDS, Strasbourg, France.

REFERENCES

Adams, F. C., Lada, C., & Shu, F. H. 1987, ApJ, 312, 788
———. 1988, ApJ, 326, 865
Adams, F. C., & Shu, F. H. 1986, ApJ, 308, 836
Alexander, D. R. 1995, private communication
Alexander, D. R., Auguson, G. C., & Johnson, H. R. 1989, ApJ, 345, 1014
Alexander, D. R., & Ferguson, J. W. 1994, ApJ, 437, 879
Bell, K. R. 1997, in preparation
Bell, K. R., Cassen, P., Klahr, H., & Henning, Th. 1997, in preparation
Bell, K. R., & Lin, D. N. C. 1994, ApJ, 427, 987
Bell, K. R., Lin, D. N. C., Hartmann, L. W., & Kenyon, S. J. 1995, ApJ, 444, 376 (BLHK)
Bessell, M. S., & Brett, J. M. 1988, PASP, 100, 1134
Bodenheimer, P., Yorke, H. W., Różyczka, M., & Tohline, J. 1990, ApJ, 355, 651
Calvet, N., Hartmann, L., & Kenyon, S. J. 1991a, ApJ, 383, 752
———. 1993, ApJ, 402, 623
Calvet, N., Patino, A., Magris, G. C., & D'Alessio, P. 1991b, ApJ, 380, 617
Cohen, M. 1980, MNRAS, 191, 499
Colina, L., & Bohlin, R. C. 1994, AJ, 108, 1931
Cox, A. N., & Tabor, J. E. 1976, ApJS, 31, 271
Eislöffel, J., Hessman, F. V., & Mundt, R. 1990, A&A, 232, 70
Hartmann, L., & Kenyon, S. 1985, ApJ, 299, 462
———. 1996, ARA&A, 34, 207
Hartmann, L., Kenyon, S., & Calvet, N. 1993a, ApJ, 407, 219
Hartmann, L., Kenyon, S., & Hartigan, P. 1993b, in Protostars and Planets III, ed. E. H. Levy & J. Lunine (Tucson: Univ. of Arizona Press), 497
Herbig, G. 1966, Vistas Astron., 8, 109
———. 1977, ApJ, 217, 693
———. 1989, in ESO Workshop on Low Mass Star Formation and Pre–Main-Sequence Objects, ed. B. Reipurth (Garching: ESO), 233
Johnson, H. L. 1965, ApJ, 141, 923
Kawazoe, E., & Mineshige, S. 1993, PASJ, 45, 715
Kenyon, S. J., Calvet, N., & Hartmann, L. W. 1993, ApJ, 414, 676
Kenyon, S. J., & Hartmann, L. W. 1987, ApJ, 323, 714
———. 1989, ApJ, 342, 1134
Kenyon, S. J., & Hartmann, L. W. 1991, ApJ, 383, 664
Kenyon, S. J., Hartmann, L. W., & Hewett, R. 1988, ApJ 325, 231
Kenyon, S. J., Hartmann, L. W., & Kolotilov, E. A. 1991, PASP, 103, 1069
Kley, W., & Lin, D. N. C. 1996, ApJ, 461, 933
Lin, D. N. C., Hayashi, M., Bell, K. R., & Ohashi, N. 1994, ApJ, 435, 821
Lin, D. N. C., & Papaloizou, J. 1985, in Protostars and Planets II, ed. D. C. Black & M. S. Matthews (Tucson: Univ. of Arizona Press), 981
Mathis, J. S. 1990, ARA&A, 28, 37
Mihalas, D. 1978, Stellar Atmospheres (2d ed.; San Francisco: Freeman)
Murdin, P., & Penston, M. V. 1977, MNRAS, 181, 657
Paczyński, B. 1976, QJRAS, 17, 31
Petrov, P. P., & Herbig, G. H. 1992, ApJ, 392, 209
Pollack, J. B., Hollenbach, D., Beckwith, S., Simonelli, D. P., Roush, T., & Fong, W. 1994, ApJ, 421, 615
Pollack, J. B., McKay, C., & Christofferson, B. 1985, Icarus, 64, 471
Racine, R. 1968, AJ, 73, 233
Reipurth, B. 1991, in IAU Symp. 137, Flare Stars in Star Clusters, Associations, and the Solar Vicinity (Dordrecht: Kluwer), 229
Ruden, S. P., & Pollack J. B. 1991, ApJ, 375, 740
Seaton, M. J., Yan, Y., Mihalas, D., & Pradhan, A. K. 1994, MNRAS, 266, 805
Shakura, N. I., & Sunyaev, R. A. 1973, A&A, 24, 337
Simon, M., Longmore, A. J., Shure, M. A., & Smillie, A. 1996, ApJ, 456, L41
Straizys, V., Meistas, E., Vansevicius, V., & Goldberg, E. P. 1989, A&A, 222, 82
Syer, D., & Clarke, C. 1996, MNRAS, 278, L23
Wooden, D. H. 1996, private communication
Wooden, D. H., Bell, K. R., Butner, H. M., & Goguen, J. D. 1995, BAAS, 187, 22.06
Yorke, H. W. 1979, A&A, 80, 308
———. 1986, in Astrophysical Radiation Hydrodynamics, ed. K.-H. Winkler & M. L. Norman (Dordrecht: Reidel), 141
Yorke, H. W., Bodenheimer, P., & Laughlin, G. 1993, ApJ, 411, 274
———. 1995, ApJ, 443, 199